Thermal conductivity of nanoscale thin nickel films*

YUAN Shiping and JIANG Peixue**

(Key Laboratory of Thermal Science and Power Engineering, Department of Thermal Engineering, Tsinghua University, Beijing 100084, China)

Received January 25, 2005; revised April 15, 2005

Abstract The inhomogeneous non-equilibrium molecular dynamics (NEMD) scheme is applied to model phonon heat conduction in thin nickel films. The electronic contribution to the thermal conductivity of the film is deduced from the electrical conductivity through the use of the Wiedemann-Franz law. At the average temperature of $T = 300$ K, which is lower than the Debye temperature $\Theta_D = 450$ K, the results show that in a film thickness range of about 1—11 nm, the calculated cross-plane thermal conductivity decreases almost linearly with the decreasing film thickness, exhibiting a remarkable reduction compared with the bulk value. The electrical and thermal conductivities are anisotropic in thin nickel films for the thickness under about 10 nm. The phonon mean free path is estimated and the size effect on the thermal conductivity is attributed to the reduction of the phonon mean free path according to the kinetic theory.

Keywords: nanoscale, nickel films, thermal conductivity, electrical conductivity.

To analyze the thermal behavior of nanosize materials and nanoelectronic devices, new physical models on the atomic scale are required. Recently, many experimental and theoretical studies have been applied to predict or measure the thermal conductance of nanowires, superlattices, thin films, and periodic thin film structures[1—5]. Recent progress in micro- and nanoscale technologies has made it possible to utilize very thin films for a variety of applications. Nickel films are of special interest because of their practical applications in ferromagnetism and their superparamagnetic behavior in microelectronic devices and microactuators[6,7]. The performance and reliability of these devices strongly depend on the heat conduction in the thin films, so the thin film thermal conductivity and the heat transport mechanism must be well understood. Recent experimental techniques, such as near-field microscopy[8,9], allow the investigation of heat transfer at small scales, but the spatial resolution is still larger than 50 nm, which remains too large when the typical length of interest is a few nanometers.

Thermal transport in metals can be analyzed from knowledge of the phonon heat transfer and the electronic heat transfer. In pure bulk metals, the phonon heat transfer will be completely swamped by the much larger electronic heat transfer[10]. But in thin metallic films, the electronic contribution to the thermal conductance decreases dramatically[11] and the thermal conductivity due to phonon heat transfer also decreases[12].

Numerical simulations can be used to predict the thermophysical properties of materials at nanoscales that cannot be experimentally measured. Molecular dynamics (MD) method is a valuable tool for studying the atomic scale properties of solids[13,14]. Classical MD methods simulate only the interaction between atomic nuclei, which means that the heat transfer due to the phonon-phonon interactions is taken into account. The success of MD simulation depends upon the accuracy of the inter-particle potential model used in simulation. This is not a problem for insulators or semiconductors in which the electronic heat transfer is negligible. Over the last two decades, several types of potential model, such as tight-binding theory[15], pseudo-potential[16], empirical potential function[17], and embedded-atom method (EAM)[18], have been developed to describe the inter-atomic interaction of metals. In transition and noble metal systems, the EAM model, originally proposed by Daw and Baskes in 1984, has been widely used to describe the energetic of metallic systems. Four different versions of EAM model provided by Johnson[19], Mei[20], Cai[21] and Pohlong[22] have hitherto been developed to employ different embedded functions, electron density functions and two-body interaction functions.

* Supported by the Specialized Research Fund for the Doctoral Program of Higher Education of China (Grant No. 20020003004) and National Fund for Distinguished Young Scholars (Grant No. 50025617)

** To whom correspondence should be addressed. E-mail: Jiangpx@mail.tsinghua.edu.cn

Among them, the versions of Johnson, Mei and Cai agree better with the data transformed from the experiments of the isobar heat capacity of Cu, Ni and Ag[23,24]. Therefore, the version of Cai is selected for computing thermal conductivity due to phonon-phonon interactions of nickel in the present study. The formulae and parameters of the EAM version are the same as those presented in the paper of Cai and Ye[21].

The thermal conductivity measurements are more difficult and inherently less accurate than electrical resistivity measurements. Therefore, the Wiedemann-Franz law is often used to convert electrical conductivity values into estimates of the thermal conductivity[10]. However, when the metallic film thickness is lower than 50 nm, thin film electrical conductivity is also extremely difficult to measure. Therefore, for very thin films, the free-electron model, Boltzmann transport equation (BTE), quantum-mechanical treatment and the *ab initio* relativistic Korringa-Kohn-Rostoker (KKR) method are used to estimate the electrical resistivity of thin metallic films[25—28].

In this study, we will calculate the electrical conductivity using the Kubo linear-response formalism, with the Wiedemann-Franz law used to relate these values to the electronic component of the thermal conductivity of the films. Estimated by using NEMD method and the elementary kinetic theory, the lattice contribution to the thermal conductivity is added to the electronic component to obtain the cross-plane thermal conductivity of the materials.

1 Electrical conductivity

In the independent-electron approximation, according to a linear-response treatment, the Hamiltonian for an electron in the presence of a semiclassical electromagnetic field characterized by vector potential $\boldsymbol{A}$. Thus[29]

$$H = \left[\frac{\hat{p}^2}{2m^*} + V(\boldsymbol{r})\right] + \left[\frac{e}{2m^* c}(\hat{p}\cdot\boldsymbol{A} + \boldsymbol{A}\cdot\hat{p})\right] \equiv [H_0] + [H_1], \quad (1)$$

where $\hat{p}$ is the momentum operator, $V(\boldsymbol{r})$ is the potential in the absence of an applied external field, $H_0 = \hat{p}^2/2m^* + V(\boldsymbol{r})$ is treated as the unperturbed Hamiltonian and m^* is the effective electron mass. In addition, assuming that the electrons are coupled to some source of dissipation, e. g. electron-electron interactions, electron-phonon interactions, magnetic scattering, etc., we introduce a relaxation time τ ($\gamma = 1/\tau$ is the corresponding relaxation rate). The equation of motion for the density matrix of electrons is

$$\frac{\partial\hat{\rho}(t)}{\partial t} + \mathrm{i}[\hat{H}(t), \hat{\rho}(t)] = -\gamma[\hat{\rho}(t) - \hat{\rho}_{\mathrm{qe}}(t)]. \quad (2)$$

Here, $\hat{\rho}_{\mathrm{qe}}$ is the quasiequilibrium density matrix and μ_0 is the chemical potential. According to the linear-response theory, the density matrix can be approximated by $\hat{\rho} \approx \hat{\rho}^{(0)} + \hat{\rho}^{(1)}$, where $\hat{\rho}^{(1)}$ is linear in the perturbation due to H_1. From Eq. (2), the off-diagonal components of the density matrix are of the form

$$\langle i | \hat{\rho}^{(1)} | j\rangle = \frac{f_i - f_j}{\varepsilon_{ij}} \frac{\varepsilon_{ij} - i\gamma}{\varepsilon_{ij} - \omega - i\gamma}\langle i | \hat{H}_1 | j\rangle, \quad (3)$$

where $\varepsilon_{ij} = \varepsilon_i - \varepsilon_j$, f_i is the Fermi-Dirac occupation factor, $|i\rangle$ and $|j\rangle$ are eigenstates of H_0.

The induced current $\boldsymbol{j}_{\mathrm{ind}}$ is obtained by $Tr\{\hat{\rho}\hat{\boldsymbol{j}}\}$. In general, the induced current is composed of two parts, one is a diamagnetic contribution arising from the change in the current operator due to the vector potential, and the other is a paramagnetic term from the off-diagonal element in the density matrix. The electrical conductivity is calculated from $\boldsymbol{j}_{\mathrm{ind}} = \sigma(\omega)\boldsymbol{E}(\omega) = \sigma(\omega)(\mathrm{i}\omega/c)\boldsymbol{A}(\omega)$. Thus

$$\sigma(\omega) = \frac{\mathrm{i}e^2}{m^*\omega}\left[\frac{N}{\Omega} + \frac{1}{\Omega m^*}\sum_{i\neq j}\frac{f_i - f_j}{\varepsilon_{ij}}\frac{\varepsilon_{ij} - \mathrm{i}\gamma}{\varepsilon_{ij} - \omega - \mathrm{i}\gamma} \times |\langle i | \hat{p}_{\mathrm{E}} | j\rangle|^2\right], \quad (4)$$

where $\langle i | \hat{p}_{\mathrm{E}} | j\rangle$ is the matrix element of the momentum operator along the applied field. The real part of the conductivity in Eq. (4) now becomes

$$\mathrm{Re}\sigma(\omega) = \frac{e^2}{(m^*)^2\Omega}\sum_{i\neq j}\frac{f_i - f_j}{\varepsilon_{ji}}\frac{\gamma}{(\varepsilon_{ij} - \omega)^2 + \gamma^2} \times |\langle i | \hat{p}_{\mathrm{E}} | j\rangle|^2. \quad (5)$$

The diamagnetic term in this case is exactly canceled by a piece from the paramagnetic term. This can be shown by invoking the well-known Thomas-Reiche-Kuhn sum rule[30], which demonstrates that the sum is independent of the choice of i,

$$\frac{2}{m^*}\sum_j \frac{|p_{ij}|^2}{\varepsilon_{ij}} = -1, \quad (6)$$

where i and j denote all the quantum numbers of a system, and the matrix elements are summed over all states j. The matrix elements of the momentum operator can next be evaluated between states $|i\rangle \equiv |k, m\rangle$ and $|j\rangle \equiv |k', m'\rangle$. The momentum operators along the y and x directions can be obtained re-

spectively:

$$\langle i \mid \hat{p}_y \mid j \rangle = (-\mathrm{i}\hbar) k_y \delta_{k,k'} \delta_{m,m'},$$
$$\langle i \mid \hat{p}_x \mid j \rangle = (-\mathrm{i}\hbar) \frac{2}{d} \frac{mm'}{m^2 - m'^2} \cdot [1 - (-1)^{m+m'}] \delta_{k,k'}. \quad (7)$$

The difference in the momentum matrix elements arises primarily from the loss of translational invariance along the x direction because of the presence of surfaces. The in-plane dc conductivity may be obtained from Eq. (7),

$$\frac{\sigma_{yy}(\omega \to 0)}{\sigma_0} = \frac{n(d)}{n_0}, \quad (8)$$

where $\sigma_0 = n_0 e^2 \tau / m^*$ is the Drude conductivity, τ is the relaxation time, $n(d)$ is the film electron density and $n_0 = k_F^3 / 3\pi^2$ is the bulk electron density. However, the intersubband coupling given in Eq. (7) leads to a very different cross-plane conductivity which is given by

$$\frac{\sigma_{xx}(\omega \to 0)}{\sigma_0} = \frac{n(d)}{n_0} - \frac{48}{\pi^2 \Gamma^2 n_c^3} \mathrm{Re} \sum_{m=1}^{n_c} m^2 (n_c^2 - m^2) \times \begin{cases} -v \tan v, & \text{if } m \text{ is even}, \\ v \cot v, & \text{if } m \text{ is odd}, \end{cases} \quad (9)$$

where $\Gamma = \gamma / \varepsilon_0$ is the level broadening in units of the zero-point energy, $n_c = \mathrm{Int}[k_F d / \pi]$ (Integer) and $v = (\pi m / 2)(1 - \mathrm{i}\Gamma / m^2)^{1/2}$. When the in-plane momentum is discrete, Eq. (9) will be consistent with the result of small metallic particles presented in Ref. [29].

For large d ($d \gg 0.18$ nm), or equivalently for $n_c \gg 1$, in which case the summation over n in the second term in Eq. (9) is approximated by an integral using Euler-Maclaurin summation formula[31]

$$\Delta = 6\sqrt{2}\beta x \int_0^1 y^2 (1 - y^2) \cdot \left[\frac{\beta}{t} + 2\mathrm{e}^{-\sqrt{2}/xt} \left(t \sin(xt) + \frac{\beta}{t} \cos(xt) \right) \right] \mathrm{d}y, \quad (10)$$

where $t = [y^2 + (y^4 + \beta^2)^{1/2}]^{1/2}$, $\beta = \hbar / \varepsilon_F \tau = 2 / k_F l$, and $x = l/d$ (l is the electron mean free path). Combined Eqs. (10), (9) and (8), the relationship between the in-plane dc σ_{yy} and cross-plane dc σ_{xx} is

$$\sigma_{xx}(\omega \to 0) = \sigma_{yy}(\omega \to 0) - \Delta \cdot \sigma_0. \quad (11)$$

As shown in Eq. (11), the electrical conductivity of metallic films is anisotropic. However, many research works are mainly focused on the in-plane electrical conductivity[25—28].

2 Electronic heat transfer

For pure metals at room temperature, from the elementary kinetic theory[32,33] and the equivalent thermal resistance schemes given in Ref. [12],

$$\frac{1}{\lambda_e} = \frac{1}{\lambda_{e\text{-ph}}}. \quad (12)$$

Here, λ_e is the thermal conductivity associated with the conduction electrons in a material and $\lambda_{e\text{-ph}}$ is the thermal conductivity due to electron-phonon interactions.

In general, λ_e is deduced from the electrical conductivity through the use of the Wiedemann-Franz law. Some researchers[34—37] expect it to be also fit for the thin metallic films. This is because it can be only invalidated by inelastic electron scattering processes. Moreover, from a transport point of view, these thin films differ from the bulk materials primarily by the elastic electron and phonon scattering centers associated with disorders in the film structure. Therefore,

$$\frac{\lambda_f}{\lambda_b} = \frac{\sigma_f}{\sigma_b}. \quad (13)$$

In thin metallic films, considering the influence of grain boundary scattering, while the grain size increases with the thickness, the average relaxation time in the film can be obtained by Matthiessen's rule[10,38],

$$\frac{1}{\tau} = \frac{1}{\tau_b} + \frac{v_F}{d_g}, \quad (14)$$

where τ_b is the electron relaxation time of the bulk crystal, v_F is the electron velocity equal to the Fermi velocity and d_g is the average in-plane grain diameter in the film. For pure nickel, in the second order of the perturbation theory in pseudo-potential and the hybridization potential, the inverse relaxation time τ_b^{-1} is[39]

$$\tau_b^{-1} = \tau_Z^{-1} + \tau_M^{-1}. \quad (15)$$

Here, the first contribution is the Ziman's relaxation time[40] from the scattering of the electrons on ions and the second contribution is the Mott's relaxation time[41]. Considering the grain boundary scattering, Kumar and Vradis[11] proposed a correlation on the in-plane thermal conductivity of thin metallic films from BTE,

$$\frac{\lambda_f}{\lambda_b} = \frac{1}{1 + B/\delta}\left[1 - \frac{3}{8}\frac{1}{B + \delta}\right],$$

$$B = \frac{d}{d_g}, \quad B + \delta > 1. \tag{16}$$

Here, d is the film thickness, $\delta = d/\Lambda_e$. Λ_e is the electron mean free path and d_g is the average grain diameter. Nath and Chopra[42] believed that the grain diameters were of the order of 100 angstroms for the film deposited at room temperature. Considering boundary scattering and grain boundary scattering, Qiu and Tien[43] developed the following approximation

$$\frac{\lambda_f}{\lambda_b} = \left[1 + \frac{3}{8}\frac{1}{\delta} + \frac{7}{5}\alpha\right]^{-1}, \quad \delta > 1 \tag{17}$$

with

$$\alpha = \frac{R}{1 - R}\frac{B}{\delta}.$$

Here, R is the reflection coefficient of the conduction electrons striking the grain boundaries ($0 \leqslant R \leqslant 1$).

3 Phonon heat transfer

To our knowledge, till now, no experimental phonon thermal conductivities for metals are available in literature. Therefore, only theoretical methods can be used to evaluate the thermal conductivity due to phonon heat transfer. For a pure metal, from the elementary kinetic theory[32,33] and the equivalent thermal resistance schemes given in Ref. [12],

$$\frac{1}{\lambda_{ph}} = \frac{1}{\lambda_{ph\text{-}ph}} + \frac{1}{\lambda_{ph\text{-}e}}. \tag{18}$$

According to the elementary kinetic theory,

$$\lambda_{ph\text{-}e} = \frac{l_{e\text{-}ph}}{l_{ph\text{-}ph}}\frac{n_{ph}}{n_e}\lambda_{ph\text{-}ph}. \tag{19}$$

The electron velocity is taken equal to the Fermi velocity $v_e = 2.04 \times 10^6\ m \cdot s^{-1}$, and the phonon velocity is equal to the sound velocity $v_{ph} = 5630\ m \cdot s^{-1}$[44]. The volume specific heat and the phonon density are calculated from the Debye model[45].

The thermal conductivity due to phonon-phonon interactions is estimated using non-equilibrium molecular dynamics (NEMD) method with the embedded-atom model (EAM). Fig. 1 is the schematic diagram for modeling steady-state heat conduction across thin films. Nickel is an fcc metal with a lattice parameter a equal to 0.352 nm. The crystal orientation is [100], [010], and [001], so the dimensions are $n_x a$, $n_y a$, and $n_z a$ in the x, y, and z directions, respectively. Periodic boundary conditions are used in the y and z directions. In the x direction, the system is confined between two hard walls at temperatures T_h and T_l, respectively; the variety of film thickness is modeled by changing the number of lattice cells in the x direction. In order to model more different thickness films, two groups of cases are studied here: (a) the lattice cell numbers in three directions are $n_x = 4$—8 and $n_y = n_z = 6$, thereby the number of atoms is $N = 576$—1152; (b) $n_y = n_z = 4$ and $n_x = 10$—30, with $N = 640$—1920.

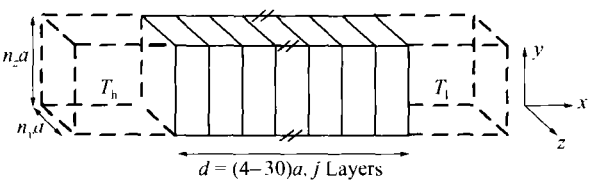

Fig. 1. Schematic diagram of model system for heat conduction normal to thin nickel films.

As shown in Fig. 1, the box is divided into several layers along the x axis. The two hard walls are maintained at $T_h = 350$ K and $T_l = 250$ K. Simulations are performed at constant density. The lattice constant is $a = 0.352$ nm, thus the film thickness ranges of the two cases are (a) $d = 1.408$—2.816 nm and (b) $d = 3.520$—10.56 nm, respectively. There are several methods to establish a temperature gradient in the system[46,47]. Here the stochastic method in Ref. [46] is applied to simulate the hard walls, treating them as hot wall and cold wall. The temperature gradient value ∇T in the normal direction of the film, and the effective thermal conductivity is determined according to Fourier's law[48],

$$\lambda_{ph\text{-}ph} = \frac{\Delta E_{k,in} + \Delta E_{k,out}}{2\tau A\,|\nabla T|}, \tag{20}$$

where A is the area perpendicular to the heat flux and d is the film thickness. Both the energy gain $\Delta E_{k,in}$ and energy loss $\Delta E_{k,out}$ across the high- and low-temperature surfaces, respectively, are instantaneously computed within every simulation step. Statistically, the relative difference between $\Delta E_{k,in}$ and $\Delta E_{k,out}$ is less than 15% in our simulations.

Since the unit cell contains 4 atoms, the number of atoms per lattice parameter in the x direction is equal to $4n_y n_z$, which is defined as a layer of atoms. Because the system undergoes nonequilibrium irreversible heat flow, local thermodynamic equilibrium should be established throughout the system when the

simulation reaches the ultimate steady state, which guarantees the validity of Eq. (20). In the present simulations, the layer number is about 4—30, the number of atoms in each layer is about 58—144, and the total simulation time is about 0.072—0.143 ns; thus the number of phonon-phonon scattering events $N_s = 3N_j\tau_{sim}/\tau_{ph}$[49] in each layer can be of the order of 10^5—10^6, which is adequate for restoring local thermodynamic equilibrium. For a set of N_j atoms in each layer, the average temperature is directly related to the kinetic energy

$$T_{MD} = \frac{m}{3N_j k_B}\left\langle \sum_{i=1,N_j} v_i^2 \right\rangle, \qquad (21)$$

where $\langle\ \rangle$ denotes the statistical averaging over all of the simulation time, k_B is the Boltzmann constant, m is the atomic mass, v_i is the velocity norm of each atom i, and N_j is the number of atoms in layer j. Eq. (21) is commonly used in MD simulations; however, it is a classical formula valid only at very high temperature ($T \gg \Theta_D$). In the present study, the system average temperature (T = 300 K) is lower than the Debye temperature (Θ_D = 450 K), it is necessary to apply a quantum correction by introducing appropriate phonon dispersion[49]. As suggested by Feng et al.[48], the real local temperature T can be deduced from T_{MD} by solving the equation

$$3N_j k_B T_{MD} = \int_0^{\omega_D} D(\omega) n(\omega, T)\, \hbar\, d\omega, \qquad (22)$$

where D is the density of states, n is the phonon occupation number, and ω is the phonon frequency. At the same time, the temperature gradient in Eq. (20) must be corrected as well.

4 Results and discussion

Compared with other metals, nickel has a smaller electrical conductivity, so the electronic component of the thermal conductivity is also lower[12]. At room temperature (T = 300 K), the thermal conductivity of bulk nickel is λ = 91.0 W·m^{-1}·K^{-1}[32]. Kumar and Vradis[11] assumed that $d \approx d_g$ was a logical one according to Nath and Chopra[42]. The values of R reported in the literature are compiled by Qiu and Tien[43]. R is chosen to be 0.19[50], and we choose B = 3.0 to match Kumar and Vradis' data. Eqs. (11), (13), (14), (16) and (17) are used to calculate the thermal conductivity due to electronic heat transfer in the nickel films. Eqs. (11) and (13) denote that the electrical conductivity and the thermal conductivity on the in-plane and cross-plane are anisotropic because of the discrete nature of the states in the film. The results in Fig. 2 show that the thermal conductivity increases with the increasing film thickness, the cross-plane conductivity is less than the in-plane conductivity for the film thickness under about 10 nm, and the difference between the in-plane and cross-plane thermal conductivities decreases with the increasing film thickness.

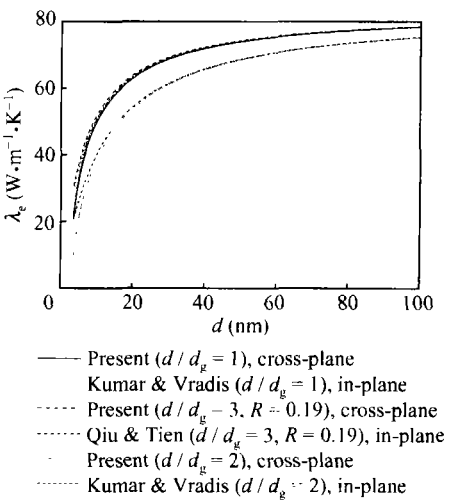

Fig. 2. The in-plane and cross-plane thermal conductivity due to electronic heat transfer as a function of film thickness.

Fig. 3 shows the calculated temperature profiles for a film with thickness $d \approx 7.04$ nm. The local instantaneous temperature calculated in each layer fluctuates more slightly with the increasing overall simulation time. However, computation of temperature distribution in nickel films is rather time consuming with the increasing overall simulation time. Fortunately, the temperature profiles can be improved by prolonging the sampling time of temperature statistics or by averaging the intermediate temperature profiles. As shown in Fig. 3, the solid lines are the average and linear fitting. By averaging the four profiles, local temperature fluctuation is effectively reduced. With the temperature quantum correction and the gradient of linear fitting, the thermal conductivity due to phonon-phonon interactions can then be calculated according to Eq. (20). Taking phonon-electron interactions into consideration, Eq. (19) is used to calculate the thermal conductivity $\lambda_{ph\text{-}e}$ before $\lambda_{ph\text{-}ph}$ is known. Fig. 4 shows the variation of the thermal conductivity due to phonon heat transfer, phonon-phonon interactions and phonon-electron interactions with the film thickness.

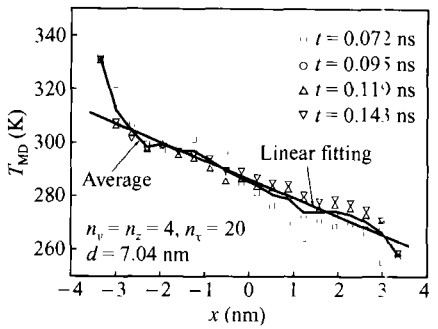

Fig. 3. Temperature distribution in the film and the influence of simulation time ($d \approx 7$ nm).

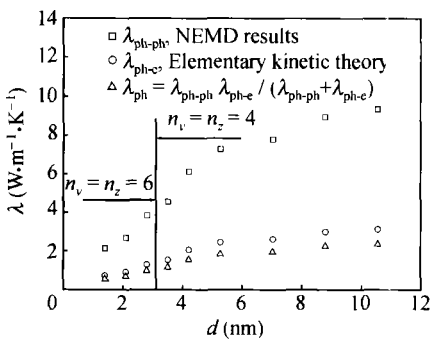

Fig. 4. Thermal conductivity due to phonon heat transfer and NEMD simulated results for various film thicknesses. The average temperature is 300 K and the temperature gradient is 100 K.

It can be seen from Fig. 4 that it is difficult to extrapolate the curve $\lambda_{ph\text{-}ph}$ to infinite thickness to give the bulk value of the thermal conductivity of nickel due to phonon-phonon interactions. A relation between the bulk value and the value obtained from MD simulation proposed by Ercolessi[51] is used to obtain the bulk value of the thermal conductivity of nickel due to phonon-phonon interactions ($\lambda_{ph\text{-}ph}(b)$)[12]. Thus

$$29.70\ \mathrm{W \cdot m^{-1} \cdot K^{-1}} < \lambda_{ph\text{-}ph}(b) < 30.83\ \mathrm{W \cdot m^{-1} \cdot K^{-1}}. \quad (23)$$

Using the elementary kinetic theory, the bulk thermal conductivity due to phonon heat transfer can be calculated

$$7.627\ \mathrm{W \cdot m^{-1} \cdot K^{-1}} < \lambda_{ph}(b) < 7.700\ \mathrm{W \cdot m^{-1} \cdot K^{-1}}. \quad (24)$$

From the result in Eq. (24), the ratio of the thermal conductivity due to phonon heat transfer to the total thermal conductivity is about 8.5%. These results are realistic, as nickel is a good electric conductor. It would probably be less than that for other metals that have a larger electrical conductivity.

The simplest theory of understanding the thermal conductivity due to phonon heat transfer of thin films is the phonon gas kinetic theory[52]. Regarding the heat carriers (i. e. phonon) in nickel as gas molecules, the lattice thermal conductivity is determined by

$$k = \frac{1}{3} C_V v l, \quad (25)$$

where C_V is the heat capacity per volume, v is the sound velocity, and l is the phonon mean free path (MFP). The bulk phonon MFP in nickel can be obtained from the kinetic theory with the Debye approximation. At $T = 300$ K, a possible bulk MFP is estimated to be $l = 1.199$—1.210 nm according to Eqs. (24) and (25). Accordingly, here $l - d$ is derived and the film thickness can be taken as the effective phonon MFP in the thin films. Therefore, Eq. (25) gives the relation $\lambda \propto d$, and this is in good agreement with the calculated results with the film thickness less than 6 nm (Fig. 5). This analysis has attributed the conductivity size effect to that the film thickness is at the same order of magnitude as the phonon MFP in nanoscale thin nickel films.

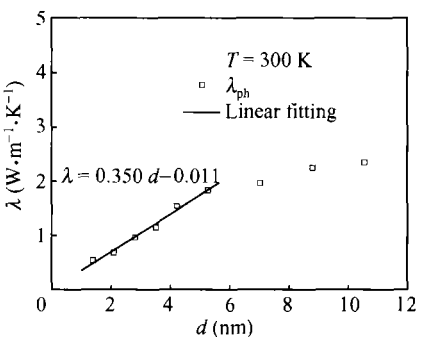

Fig. 5. Thermal conductivity due to phonon heat transfer and the theoretical results for various film thicknesses.

From the results in Figs. 2 and 4, the thermal conductivity of thin nickel films can be calculated, and the results are shown in Fig. 6. Compared with the experimental value of thermal conductivity of bulk nickel at $T = 300$ K, 91 W·m^{-1}·K^{-1}, the 3.520—10.56 nm thin film cross-plane thermal conductivity is about 2—5 times lower than that of bulk nickel, showing a remarkable boundary scattering effects, grain boundary scattering effects and size effects. However, in a nickel film thickness range of 0.4—8 μm, the experimental thin film thermal conductivity does not show apparent reduction[53]. Compared with nanoscale thin silicon films[48], the reduction of thermal conductivity in nanoscale thin metallic films

is less only because that the phonon heat transfer will be completely swamped by the much larger electron heat transfer heat in metals.

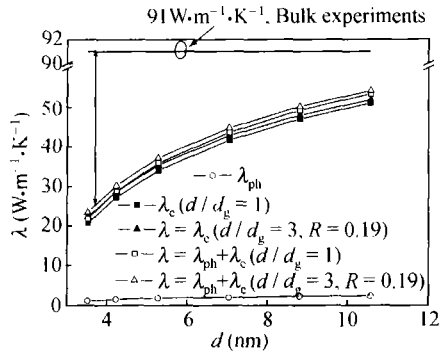

Fig. 6. Total thermal conductivity as a function of the film thickness, showing size, grain scattering and boundary effects.

5 Conclusion

The inhomogeneous NEMD scheme is appropriate for modeling heat conduction due to phonon-phonon interactions in nanoscale thin nickel films. In this paper, the thermal conductivity due to phonon heat transfer has been calculated by MD simulation and the elementary kinetic theory, the electronic contribution to the thermal conductivity of the film has been deduced from the electrical conductivity through the use of the Wiedemann-Franz law. The electrical conductivity of thin nickel films has been estimated from the Kubo linear-response formalism. We find that the cross-plane thermal conductivity of nanoscale thin nickel films has remarkable boundary scattering effects, grain boundary scattering effects and size effects, which considers electrons only at the Fermi level and at a temperature lower than the Debye temperature. In a film thickness range of 1.408—10.56 nm, the thin film cross-plane thermal conductivity is several times lower than that of bulk nickel at corresponding temperatures and decreases almost linearly as the film thickness is reduced. The electrical and thermal conductivities are anisotropic in thin nickel films with thickness under about 10 nm because of the discrete nature of the states in the system. The phonon size effect occurs because the effective phonon MFP is reduced when the film thickness is comparable to or even smaller than the phonon MFP in bulk nickel. The presence of columnar microstructures, microcracks, microgrooves, defects, impurities and dislocations may also further influence the film thermal and electrical conductivity[54,55].

References

1 Cahill D. G., Goodson K. and Majumdar A. Thermometry and thermal transport in micro/nanoscale solid-state devices and structures. Journal of Heat Transfer, 2002, 124(2): 223—241.

2 Chen G. and Shakouri A. Heat transfer in nanostructures for solid-state energy conversion. Journal of Heat Transfer, 2002, 124(2): 242—252.

3 Lukes J. R., Li D. Y., Liang X. G. et al. Molecular dynamics study of solid thin-film thermal conductivity. Journal of Heat Transfer, 2000, 122(3): 536—543.

4 Kulish V. V., Lage J. L., Komorov P. L. et al. A fractional-diffusion theory for calculating thermal properties of thin films from surface transient thermoreflectance measurements. Journal of Heat Transfer, 2001, 123(6): 1133—1138.

5 Wang X., Hu H. and Xu X. Photo-acoustic measurement of thermal conductivity of thin films and bulk materials. Journal of Heat Transfer, 2001, 123(1): 138—144.

6 Judy J. W. and Muller R. S. Magnetically actuated, addressable microstructures. Journal of Microelectromechanical Systems, 1997, 6(3): 249—256.

7 Liang M. W., Hsieh T. E., Chen C. C. et al. Electroless copper/nickel films deposited on AlN substrates. Japanese Journal of Applied Physics, 2004, 43(12): 8258—8266.

8 Majumdar A. Scanning thermal microscopy. Annual Review of Materials Science, 1999, 29(1): 505—585.

9 Fournier D., Forget B. C., Boue C. et al. Micron scale thermal imaging. International Journal of Thermal Science, 2000, 39(4): 514—518.

10 Myers H. P. Introductory Solid State Physics. London: Taylor & Francis, 1990.

11 Kumar S. and Vradis G. C. Thermal conductivity of thin metallic films. Journal of Heat Transfer ASME, 1994, 116: 28—34.

12 Chantrenne P., Raynaud M., Baillis D. et al. Study of phonon heat transfer in metallic solids from molecular dynamic simulations. Microscale Thermophysical Engineering, 2003, 7: 117—135.

13 Allen M. P. and Tildesley D. J. Computer Simulation of Liquid. New York: Oxford University Press, 1987.

14 Frenkel D. and Berend S. Understanding Molecular Simulation. San Diego: Academic Press, 1996.

15 Papadia S., Piveteau B. and Spanjaard D. Structural stability of adatom islands on fcc(111) transition-metal surfaces. Physical Review B, 1996, 54: 14720—14727.

16 Harrison W. A. Pseudopotentials in the Theory of Metals. New York: Benjamin, 1966.

17 ERKOÇ Ş., GÜNEŞ B. and GUNEŞ P. Molecular-dynamics simulations of nickel clusters. International Journal of Modern Physics C, 2000, 11(5): 1013—1024.

18 Daw M. S. and Baskes M. I. Embedded-atom method: Derivation and application to impurities, surface, and other defects in metals. Physical Review B, 1984, 29: 6443—6453.

19 Johnson R. A. Analytic nearest-neighbor model for fcc metals. Physical Review B, 1988, 37: 3924—3931.

20 Mei J., Davenport J. W. and Fernando G. W. Analytic embedded-atom potentials for fcc metals: Application to liquid and solid copper. Physical Review B, 1991, 43: 4653—4658.

21 Cai J. and Ye Y. Y. Simple analytical embedded-atom-potential model including a long-range force for fcc metals and their alloys. Physical Review B, 1996, 54: 8398—8410.

22 Pohlong S. S. and Ram P. N. Analytic embedded atom method potentials for fcc-centered cubic metals. J. Mater. Res., 1998, 13: 1919—1927.

23 Sadigh B. and Grimvall G. Molecular-dynamics study of thermodynamical properties of liquid copper. Physical Review B, 1996, 54: 15742—15746.

24 Wang J. Z., Chen M. and Guo Z. Y. Structural and thermodynamic properties of liquid transition metals with different embedded-atom method models. Chin. Phys. Lett., 2002, 19: 324—326.

25 Camblong H. E. and Levy P. M. Electrical resistivity of a thin metallic film. Physical Review B, 1999, 60: 15782—15789.

26 Zhang X. G. and Butler W. H. Conductivity of metallic films and multilayers. Physical Review B, 1995, 51: 10085—10103.

27 TeŠanović Z., Jarić M. V. and Maekawa S. Quantum transport and surface scattering. Physical Review Letters, 1986, 57: 2760—2763.

28 Blass C., Weinberger P., Szunyogh L. et al. *Ab initio* calculations of magnetotransport for magnetic multilayers. Physical Review B, 1999, 60: 492—501.

29 Wood D. M. and Ashcroft N. W. Quantum size effects in the optical properties of small metallic particles. Physical Review B, 1982, 25: 6255—6274.

30 Bethe H. and Salpeter E. Quantum Mechanics of One- and Two-Electron Atoms. Berlin: Springer, 1957.

31 Bender C. M. and Orzag S. A. Advanced Mathematical Methods for Scientists and Engineers. New York: McGraw Hill, 1978.

32 Kittel C. Introduction to Solid State Physics. New York: Wiley, 1996.

33 Ashcroft N. W. and Mermin N. D. Solid State Physics. Fort Worth: Harcourt College Publishers, 1976.

34 Anderson R. J. The thermal conductivity of rare-earth-transition-metal films as determined by the Wiedemann-Franz law. J. Appl. Phys., 1990, 67(11): 6914—6916.

35 Tien C. L., Armaly B. F. and Jagannathan P. S Thermal conductivity of thin metallic films and wires at cryogenic temperatures. In: Thermal Conductivity, Plenum Pess., 1969, 13—19.

36 Tellier C. R. and Tosser A. J. Size Effects of Thin Films. New York: Elsevier Publishing, 1982.

37 Mott N. F. and Jones H. The Theory of Properties of Metals and Alloys. New York: Dover, 1958, 305.

38 Bass J., Pratt W. P. and Schroeder P. A. The temperature dependent electrical resistivities of the alkali metals. Reviews of Modern Physics, 1990, 62: 645—744.

39 Shvets V. T., Savenko S. V. and Datsko S. V. The electroconductivity of the liquid alloys of transition metals. Condensed Matter Physics, 2004, 7: 275—284.

40 Ziman J. M. A theory of electrical properties of liquid metals, I. The monovalent metals. Phil. Mag., 1961, 6: 1013—1034.

41 Mott N. F. The electrical resistivity of liquid transition metals. Phil. Mag., 1972, 26: 1249—1261.

42 Nath P. and Chopra K. L. Thermal conductivity of copper films. Thin Solid Films, 1974, 20: 53—62.

43 Qiu T. Q. and Tien C. L. Size effect on non-equilibrium laser heating of metal films. In: Micromechanical Systems, ASME DSC, 1992, 40: 227—242.

44 Swartz E. T. and Pohl R. O. Thermal boundary resistance. Reviews of Modern Physics, 1989, 61(3): 605—668.

45 Yuan S. P. and Jiang P. X. Molecular dynamics study on thermal conductivity of nanoscale thin metallic films. In: Proceedings of the 7th Asian Thermophysical Properties Conference. Hefei & Huangshan, Anhui, China, August 23—29, 2004.

46 Tenenbaum A., Ciccotti G. and Gallico R. Stationary nonequilibrium states by molecular dynamics: Fourier's law. Physical Review A, 1982, 25: 2778—2787.

47 Ikeshoji T. and Hafskjold B. Non-equilibrium molecular dynamics calculation of heat conduction in liquid and through liquid-gas interface. Molecular Physics, 1994, 81: 251—261.

48 Feng X. L., Li Z. X. and Guo Z. Y. Molecular dynamics simulation of thermal conductivity of nanoscale thin silicon films. Microscale Thermophysical Engineering, 2003, 7: 153—161.

49 Maiti A., Mahan G. D. and Pantelides S. T. Dynamical simulations of nonequilibrium process-heat flow and the Kapitza resistance across grain boundaries. Solid State Communications, 1997, 102: 517—521.

50 De Vries J. W. C. Temperature-dependent resistivity measurements on polycrystalline Sio2-covered thin nickel films. Thin Solid Films, 1987b, 150: 209—215.

51 Ercolessi F. A Molecular Dynamics Primer, International School for Advanced Studies (SISSA-ISAS), Spring College in Computational Physics, ICTP. Italy: Trieste, 1997.

52 Ziman J. M. Electrons and Phonons. London: Oxford University Press, 1960.

53 Langer G., Hartmann J. and Reichling M. Thermal conductivity of thin metallic films measured by photothermal profile analysis. Rev. Sci. Instrum., 1997, 68(3): 1510—1513.

54 Wu Z. L., Kuo P. K., Wei L. H. et al. Photothermal characterization of optical thin films. Thin Solid Films, 1993, 236: 191—198.

55 Redondo A. and Beery J. G. Thermal conductivity of optical coatings. Journal of Applied Physics, 1986, 60: 3882—3885.